# Confined space self-propagating room temperature synthesis of carbon-encapsulated $Fe_3O_4$ nanocrystals and its lithium storage performance

IOP Publishing Nanotechnology
Nanotechnology 30 (2019) 435603 (11pp) https://doi.org/10.1088/1361-6528/ab3312

# Confined space self-propagating room temperature synthesis of carbon-encapsulated $Fe_3O_4$ nanocrystals and its lithium storage performance

**Boyang Liu[1,4], Shuyu Ke[1], Jianwei Lin[2,4], Yuliang Zhang[1], Xiqin Zhang[1], Shengchang Yan[1], Qi Yu[1] and Yingfeng Shao[3]**

[1] College of Ocean Science and Engineering, Shanghai Maritime University, Shanghai 201306, People's Republic of China
[2] College of Marine Ecology and Environment, Shanghai Ocean University, Shanghai 201306, People's Republic of China
[3] State Key Laboratory of Nonlinear Mechanics, Institute of Mechanics, Beijing 100190, People's Republic of China

E-mail: byliu@shmtu.edu.cn, jwlin@shou.edu.cn, 423782932@qq.com(Shuyu Ke), ylzhang@shmtu.edu.cn, xqzhang@shmtu.edu.cn, yanshengchang123@qq.com, 476821830@qq.com(Qi Yu) and shaoyf@lnm.imech.ac.cn

Received 28 April 2019, revised 25 June 2019
Accepted for publication 17 July 2019
Published 12 August 2019

**Abstract**

A self-propagating reaction between ferrocene and iron nitrate nonahydrate that is initiated at room temperature is discovered. Amorphous carbon-encapsulated $Fe_3O_4$ nanocrystals ($Fe_3O_4$@C) can be one-step prepared in an autoclave through this reaction. The equiaxed $Fe_3O_4$ nanocrystals have typical dimensions in the range of 5–60 nm with a median size of 24.1 nm, and their weight percent is up to 82.3%. The course of the reaction is recorded, and the formation mechanism of $Fe_3O_4$@C with the core–shell structure is proposed. The scaling-up synthesis is also achieved, and 52.1 g of the $Fe_3O_4$@C can be obtained in a single batch. The shock wave appeared in the fast gas release self-propagating reaction in confined space plays a decisive role in the preparation of homogeneous $Fe_3O_4$@C with a core–shell structure. The $Fe_3O_4$@C anode shows excellent capacity retention with a high specific capacity of 494 mAh $g^{-1}$ at 1 A $g^{-1}$ in the 200th cycle.

Supplementary material for this article is available online

Keywords: carbon-encapsulated $Fe_3O_4$ nanocrystals, core–shell, self-propagating synthesis, lithium-ion batteries

(Some figures may appear in colour only in the online journal)

## 1. Introduction

Carbon-encapsulated $Fe_3O_4$ nanocrystals ($Fe_3O_4$@C) improves the distinctive properties over its single components and has broad range applications such as energy storage, optical devices, drug delivery, recyclable catalyst support and is adsorbent [1–3]. However, its practical application is still restrained by the complicated laboratory-scale preparation process with high cost and low throughput [4]. In this case, hydrothermal treatment can be regarded as the simplest strategy at present and intensively utilized for one-step preparation of $Fe_3O_4$@C, generally using ferric salts and glucose as the precursors [5]. The glucose can dehydrate and aromatize, and eventually convert to a carbon shell below

[4] Authors to whom any correspondence should be addressed.

 

200 °C, which is a very low operating temperature for preparing carbon nanomaterials. But the long dwelling time and the unsatisfied microstructure homogeneity are the main constraints for scale-up fabrication. Therefore, ongoing research efforts are still needed to develop a time-effective, low energy consumption and inexpensive method for industrial-scale mass production. In our previous publications, a common oxidation route is proposed for the synthesis of carbon-encapsulated nanocrystals via a moderate detonation reaction of the organometallic compounds with oxidants below 200 °C [6–8]. The synthetic approach involves the oxidation removal of hydrogen from the organics and *in situ* generation of carbon shell. It is speculated that the stronger oxidant is inclined to further reduce the reaction temperature, and thus iron nitrate nonahydrate ($Fe(NO_3)_3 \cdot 9H_2O$) is used instead to react with ferrocene ($Cp_2Fe$) in this paper. It is surprisingly found that the reaction can take place at room temperature with large amounts of heat and gas release, leading to a quite simple procedure to form $Fe_3O_4$@C in an autoclave. We also prove that the $Fe_3O_4$@C is a high-performance anode material for lithium-ion batteries owing to its excellent cycling stability and rate capability.

## 2. Experimental section

### 2.1. Sample preparation

The operation procedure is quite simple and easy to handle. Typically, 5 mmol of $Cp_2Fe$ and 6.25 mmol of $Fe(NO_3)_3 \cdot 9H_2O$ were placed in a 50 ml autoclave with a maximum pressure of 10 MPa and kept at room temperature (*ca.* 32 °C) for 30 min. Then, the resulting powder was rinsed with ethanol, magnetically isolated and finally dried at 80 °C.

The mass production of the $Fe_3O_4$@C was also carried out. 46.5 g of $Cp_2Fe$ and 126 g of $Fe(NO_3)_3 \cdot 9H_2O$ were mixed and put into a 5 l autoclave, which was kept at room temperature for 30 min. During this process, a strongly exothermic reaction took place with a sudden pressure increase and a rapid temperature rise. After cooling down, the black powder was collected and washed with deionized water. Finally, 52.1 g of $Fe_3O_4$@C was obtained in a single batch.

### 2.2. Characterization

The phase structure of the $Fe_3O_4$@C was characterized by an x-ray PANalytical X'Pert PRO diffractometer (XRD) with a Cu $K_\alpha$ source and a Bruker micro Raman spectrometer with a 532 nm excitation, respectively. The surface morphology and elemental analysis were investigated by a JEOL JSM 7500F scanning electron microscope (SEM) with an attached EDAX energy dispersive spectrometer (EDS). The microstructure was visualized by a JEM 2010 transmission electron microscope (TEM). Differential scanning calorimetry (DSC) and thermogravimetric (TG) analysis were carried out on a simultaneous thermal analyzer NETZSCH 449 F3 with a ramp rate of 5 °C $min^{-1}$ at ambient atmosphere to determine the carbon content in the $Fe_3O_4$@C. NETZSCH DSC 204F1 was also employed to analyze the reaction of the starting materials in the autoclave using a sealed aluminum pan. The thermal behavior during the reaction was recorded by an FLIR E40 thermal imaging camera. The main components of the exhaust gas in the autoclave were measured by a flue gas analyzer (MRU Vario Plus, Germany).

### 2.3. Electrochemical measurement

As the active material, 80 wt% $Fe_3O_4$@C was evenly mixed with 10 wt% Super P carbon black and 10 wt% polyvinylidene difluoride (PVDF) in N-methyl-2-pyrrolidone (NMP) for 24 h. The homogeneous slurry was then coated on the Cu foil, which was dried in a vacuum at 120 °C for the following coin cell assembling in the Ar-filled glovebox. The mass loading of the $Fe_3O_4$@C on the foil was about 2 mg $cm^{-2}$. The lithium foil and microporous polypropylene film was used as the counter electrode and separator, respectively. The electrolyte was made up of 1.0 M $LiPF_6$ in a solution of ethylene carbonate (EC)/diethylene carbonate (DEC) (1:1 by volume) with 8 wt% fluoroethylene carbonate (FEC). The cycling stability and rate performance of the cells were measured at 25 °C using a Neware battery testing equipment in the voltage of 0.01–3 V. The cyclic voltammogram (CV) was recorded on an electrochemical workstation (CHI 630 A) at a scan rate of 0.5 mV $s^{-1}$ between 0.01 and 3 V. After the cycling test, the coin cell discharged at a current density of 1 A $g^{-1}$ was disassembled in an argon-filled glovebox, and the activated material was rinsed with an electrolyte and taken out for the SEM and TEM observation.

## 3. Results and discussion

The as-prepared powder dispersed in an aqueous solution can be vertically attracted by a magnetic bar due to the existence of $Fe_3O_4$ phase in the powder (figure S1, supplementary material is available online at stacks.iop.org/NANO/30/435603/mmedia), which can be obviously proved by the sharp characteristic diffraction peaks of cubic phase $Fe_3O_4$ (JCPDS card no. 19-0629) in the XRD pattern (figure 1(a)). However, there are not carbon diffraction peaks in this profile, suggesting that no crystalline carbon is formed in the process on account of the low inner reactor temperature and short reaction time during the synthesis. And the typical high-intensity D-band in the Raman spectrum clearly demonstrates that the carbon shell is amorphous (figure 1(b)). SEM images indicate the agglomerated nanoparticles are the major product and have core–shell structure due to the obvious white cores under the carbon layer (figures 1(c) and (d)). The EDS spectrum of these nanoparticles in the SEM image further confirms that Fe, O and C are the only elements in the powder C (figure 1(e)), corresponding well to the $Fe_3O_4$@C. The DSC-TG curves of the $Fe_3O_4$@C in air are shown in figure 1(f). The 14.2% weight loss started at about 335 °C associated with a strong exothermal peak is owing to the complete oxidation of carbon shell and the simultaneous oxidation of $Fe_3O_4$ to $Fe_2O_3$. On the basis of the remaining

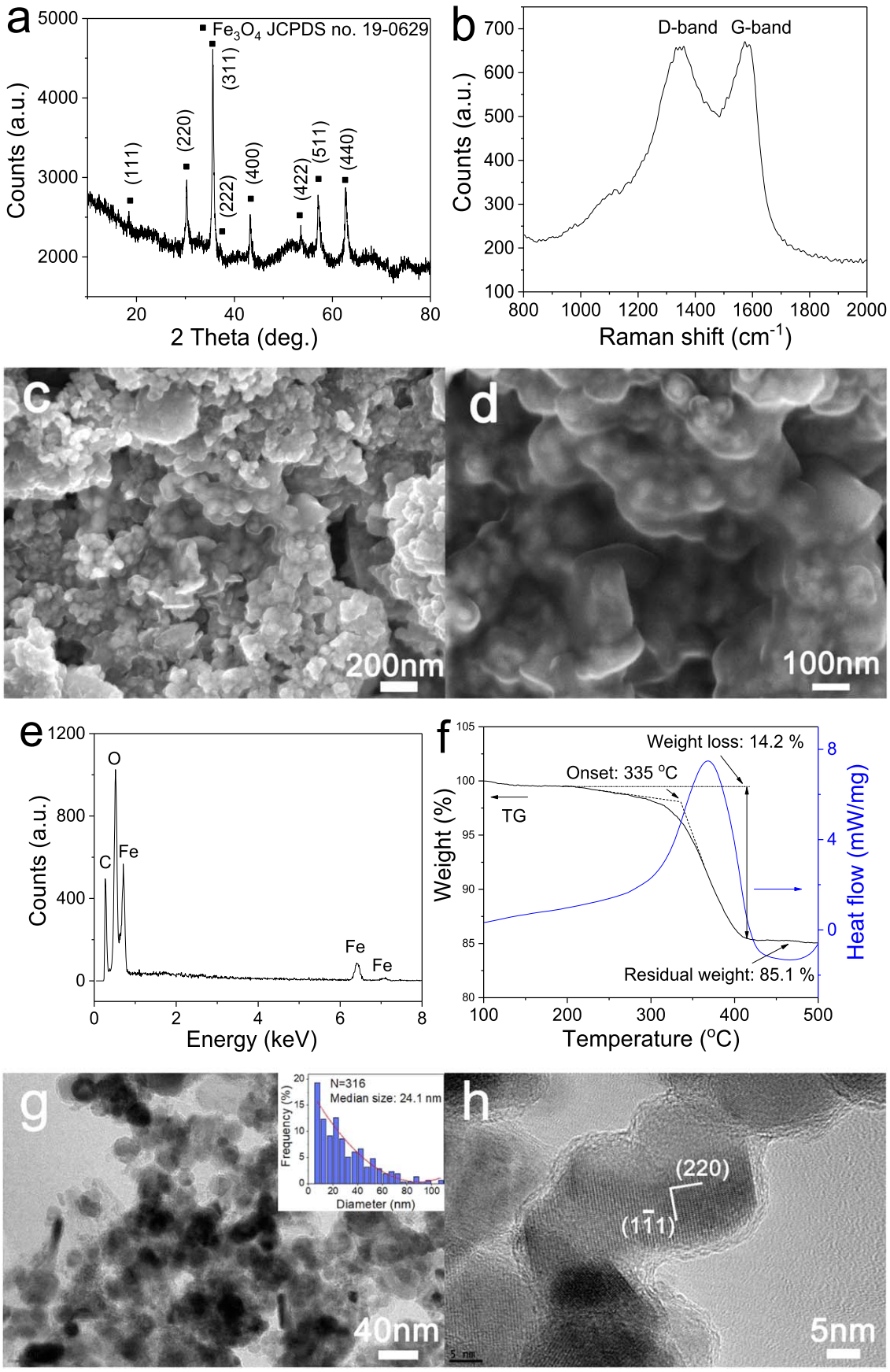


**Figure 1.** (a) XRD pattern, (b) Raman spectrum, (c), (d) SEM images, (e) EDS spectrum, (f) DSC-TG curves at ambient atmosphere, (g), (h) TEM images with size distribution histogram (inset) of the $Fe_3O_4$@C.

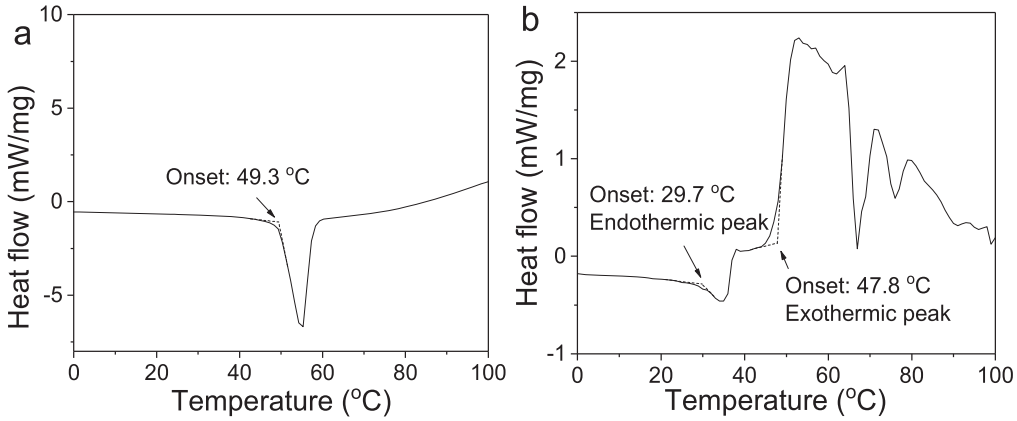


**Figure 2.** DSC curves of (a) pure $Fe(NO_3)_3 \cdot 9H_2O$ and (b) the reactants in sealed pans.

85.1 wt% of $Fe_2O_3$ after the complete reactions of $Fe_3O_4$@C in the TG curve, the content of $Fe_3O_4$ nanocrystals in the nanocomposite is calculated to be 82.3 wt%. Thus, the carbon content should be 17.7 wt%. On the assumption that the carbon and Fe atoms in the reactants are completely converted to $Fe_3O_4$@C, the weight percent of carbon in the resulting powder should be as high as 40.9 wt%. It indicates that the cyclopentadienyl rings in ferrocene partially burn as fuels to maintain the self-sustainable reaction. As a result, the $Fe_3O_4$ content is relatively high in the nanocomposite, which has a favorable effect on improving the theoretical capacity of the anode material. The TEM image of figure 1(g) reveals that most nanocrystals have an equiaxed morphology mainly concentrated in the 5–60 nm. The median crystal size is 24.1 nm as derived from the cumulative size distribution curve. The thin amorphous carbon shell of 2 nm with disordered carbon fringes is distinctly observed on the $Fe_3O_4$ nanocrystals (figure 1(h)). Accordingly, the simple method is valid for one-step preparation of the $Fe_3O_4$@C.

The DSC curve of pure $Fe(NO_3)_3 \cdot 9H_2O$ in the sealed pan is displayed in figure 2(a). The onset point of the endothermic peak is about 49.3 °C, corresponding well to the melting point of $Fe(NO_3)_3 \cdot 9H_2O$. However, the reaction behavior of $Cp_2Fe$ with $Fe(NO_3)_3 \cdot 9H_2O$ is quite different, as shown in figure 2(b). The endothermic peak has an onset point of 29.7 °C, which is much lower than the melting point of pure $Fe(NO_3)_3 \cdot 9H_2O$, hence illustrating that the reaction can take place at room temperature. In fact, the colorless $Fe(NO_3)_3 \cdot 9H_2O$ particles will very rapidly become dark blue spherical droplets when in contact with $Cp_2Fe$ powder owing to the fast oxidation of yellow $Cp_2Fe$ to blue $Cp_2FeNO_3$ (figure S2) [9, 10]. The $Cp_2FeNO_3$ is soluble in water and the solution color switches from blue to dark depending on its concentration, as evidenced by the course of dissolution in figure S3. Therefore, it is suggested that the $Cp_2FeNO_3$ will dissolve in the hydrated melt phase and dispersed as droplets, corresponding to the endothermic peak. With the temperature increases, the strong exothermic peak started at 47.8 °C should be attributed to the subsequent oxidation of the dissolved $Cp_2Fe^+$.

The detailed formation mechanism in an open bottle is discussed according to the real-time video image capture, as shown in figure 3. During the mixing, the reactant powder mixture immediately turned dark and sticky (figure 3(a1)), corresponding to an endothermic reaction indicated by the blue lower-temperature area at the bottom (figure 3(a2)). Then, the mixture gradually melted and consistently absorbed heat, which is in accordance with the DSC result (figures 3(b1), (b2)). After 600 s, the temperature of the melted mixture began to self-increase and locally reached a maximum value of 39.3 °C at 670 s (figures 3(c1)–(d2)). It is considered that the $Cp_2Fe^+$ molecule would be cleaved by the strong oxidant, and the Cp ligand underwent oxidation so as to yield heat during this period. In the following several seconds, an exothermic eruption was drastically initiated by the cumulative heat with large amounts of heat and gas released (figures 3(e1)–(f2)). The reddish-brown gas that had a characteristic biting odor could be deemed as $NO_2$. The highest bottle temperature rapidly rose to 324 °C at 690 s and immediately cooled down to 240 °C at 717 s (figure S4). These observations prove that it can be referred to as self-propagating synthesis conducted at room temperature. After reactants mixing and melting, some parts of the sample were locally heated by the oxidation-induced reaction, and then a wave of exothermic reaction was thermally activated and fast swept through the remaining material. When the reaction took place in an autoclave, the large amount of heat and gases were confined in the space and cannot be released to the external environment, probably forming a propagating shock wave. The inner sudden high pressure and temperature would completely destroy the liquid intermediate phase into reactive radical species, which self-assembly transformed into the core–shell structure [11]. In addition, when the strong nitrate radical oxidized the hydrogen in the Cp ligand, the carbon shell was well preserved because the inadequate oxygen content in the autoclave and short high-temperature dwelling time could significantly alleviate its further oxidation. The small $Fe_3O_4$ nanocrystals were obtained associated with the minimized diffusion at the relatively low temperature. The carbon shell surrounding the $Fe_3O_4$ nanocrystals also inhibited the crystal growth. Consequently, the synthesis schematic is summarized in figure 4. After the synthesis, an exhaust gas stream of CO, $CO_2$, NO, $NO_x$ and $NO_2$ was qualitatively detected while evacuating the autoclave (figure S5). In

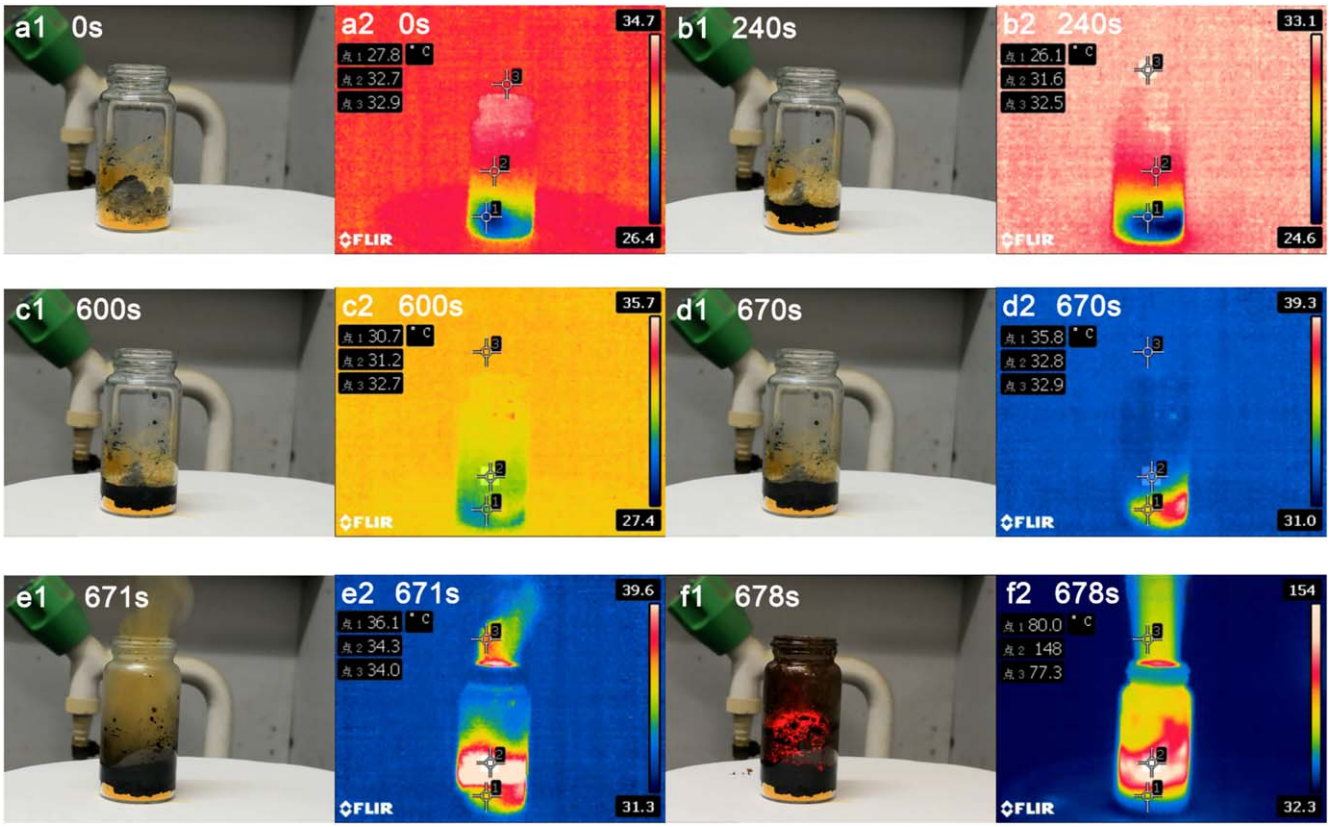


**Figure 3.** The reaction behavior in an open bottle recorded by video image capture. (a1), (b1), (c1), (d1), (e1), (f1) The optical photographs. (a2), (b2), (c2), (d2), (e2), (f2) The thermal images.

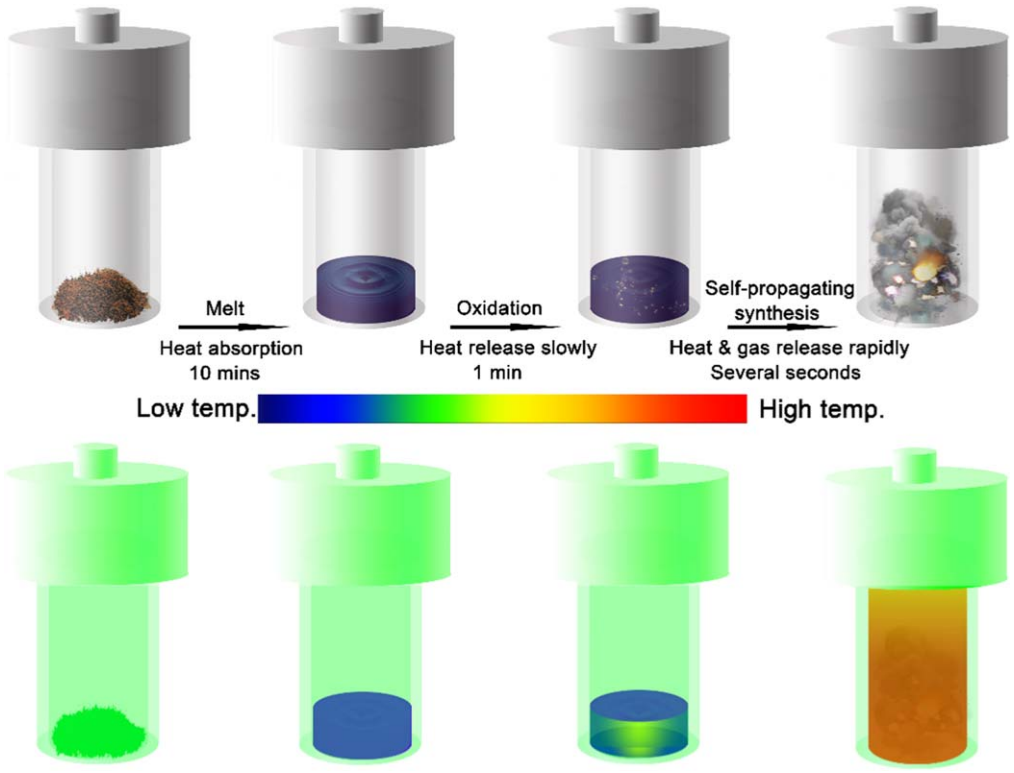


**Figure 4.** The synthesis schematic of the $Fe_3O_4$@C.

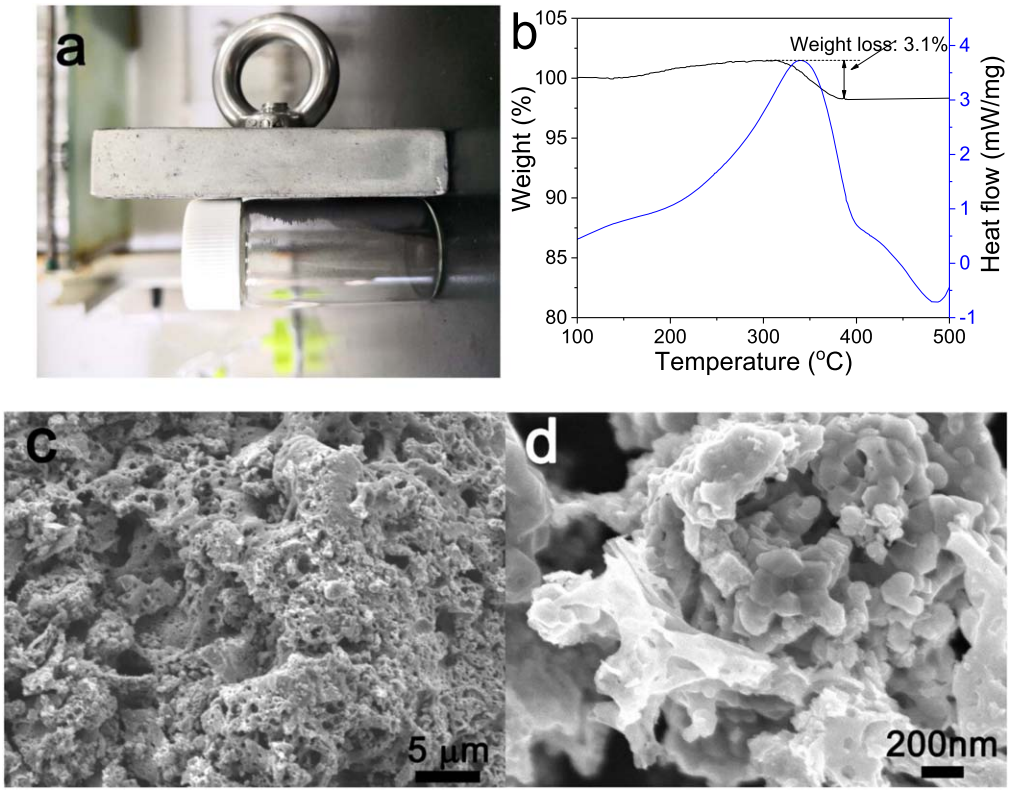


**Figure 5.** (a) The powder prepared in an open bottle was attracted by a magnet bar. (b) The DSC-TG curves of the powder carried out in air. (c), (d) The SEM images of the as-prepared powder at different magnifications.

addition, a strong ammonia smell was identified after opening the autoclave, meaning that the nitrate radical was markedly reduced in the reaction. The whole chemical equation is proposed as follows:

$$(C_5H_5)_2Fe + Fe(NO_3)_3 \cdot 9H_2O \rightarrow Fe_3O_4@C + H_2O + NH_3 + CO_x + NO_x.$$

When the synthesis was carried out in an open bottle at ambient atmosphere, the as-prepared black powder could also be totally attracted by a magnet bar (figure 5(a)), implying that $Fe_3O_4$ formed through the self-propagating reaction. However, the DSC-TG curves in figure 5(b) carried out in air reveal that the powder weight loss during the oxidation is only 3.1%, demonstrating the carbon content is very low in the powder. Therefore, most carbon had been oxidized in the synthesis process because the highest temperature was a little higher for amorphous carbon burning in the oxygen-rich atmosphere. The low magnification SEM image in figure 5(c) shows that the powder has a porous sponge-like morphology, owing to the large amount of gases escaping and short combustion duration. And the powder actually consists of agglomerated equiaxed and irregular-shaped interconnected nanoparticles with a size larger than 100 nm according to high magnification image (figure 5(d)). The morphology of the $Fe_3O_4$ nanoparticles fabricated in the open bottle is highly similar to those prepared by the conventional low temperature sol-gel combustion reaction of iron nitrate nonahydrate with citric acid, urea or glycine at ambient atmosphere [12–14]. Thus, the sample uniformity was not good using the open vessel and the $Fe_3O_4$ nanoparticles tended to grow larger without the carbon shell. Conversely, in an autoclave, the shock wave with large energy would completely break down the reactants into small atomic radical species, which uniformly filled the entire space blown by the large amount of gases and subsequently recombined for the core–shell structure. The process is very much identical to the detonation synthesis in the sealed vessel for the appropriate generation of small equiaxed nanocrystal cores with carbon shell, because both the nucleation and crystal growth take place in a very short time at a high temperature and pressure [15]. In summary, this self-propagating reaction between $Cp_2Fe$ and $Fe(NO_3)_3 \cdot 9H_2O$ with a formation of shock wave in the confined space plays a decisive role for the preparation of homogeneous $Fe_3O_4$@C. But the size uniformity of the $Fe_3O_4$ nanocrystals and carbon shell is currently difficult to control since the reaction is fairly violent and completed in a very short time. It is speculated that the more reactants in the confined space, the larger $Fe_3O_4$ nanocrystals and thicker carbon shell will be obtained. When the weight of the reactants is increased, the reaction becomes more violent and the adiabatic combustion temperature in the autoclave will be greatly raised, which favors the crystal growth. Moreover, the large quantity of radical species in the confined space will frequently collide with each other and aggregate together for a large-size core–shell structure. However, huge gas emission in the reaction leads to a high pressure in the autoclave and safety should be a primary concern.

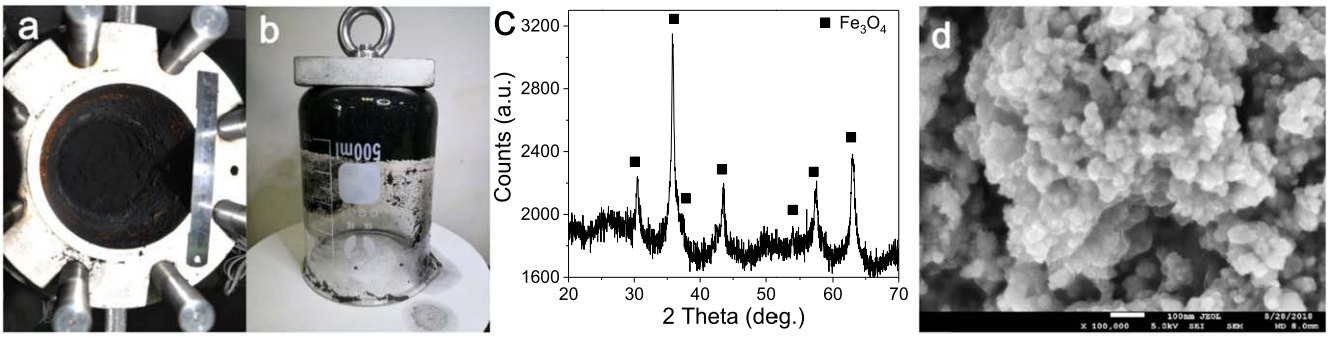


**Figure 6.** (a), (b) The photographs of the as-prepared $Fe_3O_4$@C fabricated in a 5 l autoclave. (c) The XRD pattern and (d) the SEM image of the $Fe_3O_4$@C.

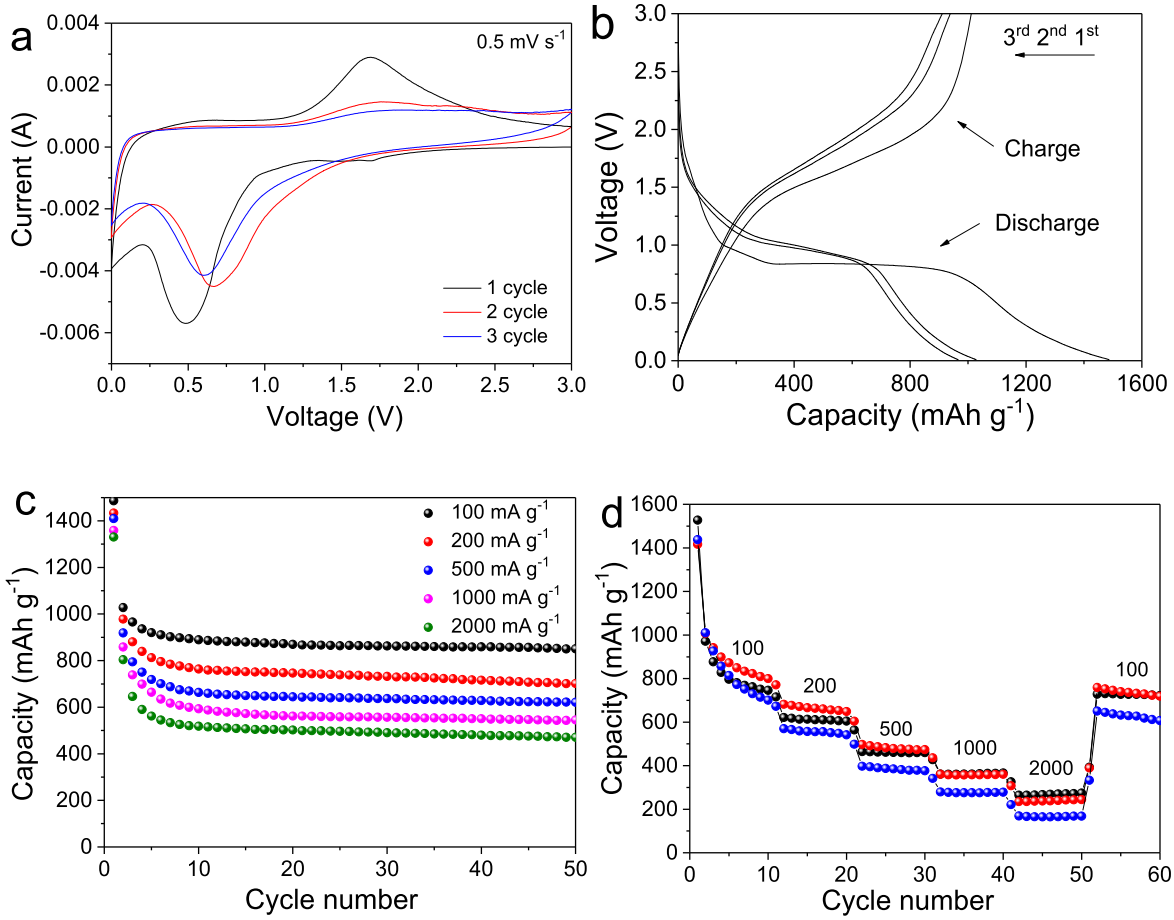


**Figure 7.** The electrochemical properties of the $Fe_3O_4$@C anodes for lithium-ion batteries. (a) CV curve; (b) the initial three voltage profiles at a current density of 100 mA $g^{-1}$; (c) the discharge capacity at different current densities; (d) the discharge capacity of three individual cells at various rates.

Based on the typical self-propagating reaction, the synthesis procedure is able to be handled in ambient condition at about room temperature. To the best of our knowledge, it is the lowest initial reaction temperature to form carbon shell regardless of the oxygen in the reactor. Since the heating source is not essential, only a temperature-resistant pressure vessel is adequate for the very short-time reaction. The scaling-up synthetic parameters are unaffected as exemplified by the mass fabrication of 52.1 g of $Fe_3O_4$@C via the reaction of 46.5 g of $Cp_2Fe$ and 126 g of $Fe(NO_3)_3 \cdot 9H_2O$ in a 5 l autoclave in 30 min (figures 6(a) and (b)). During the synthesis, the pressure in the autoclave firstly suddenly rose to nearly 8 MPa, then the inner temperature rapidly increased to a maximum value of 184 °C in 1 min due to the considerable heat liberated by the strongly exothermic reaction (video 1). It is further proved that a shock wave can appear in the fast gas release self-propagating reaction conducted in the confined space, which is helpful for the formation of core–shell structure. The corresponding XRD and SEM results are shown in figures 6(c) and (d). The $Fe_3O_4$ nanocrystals and

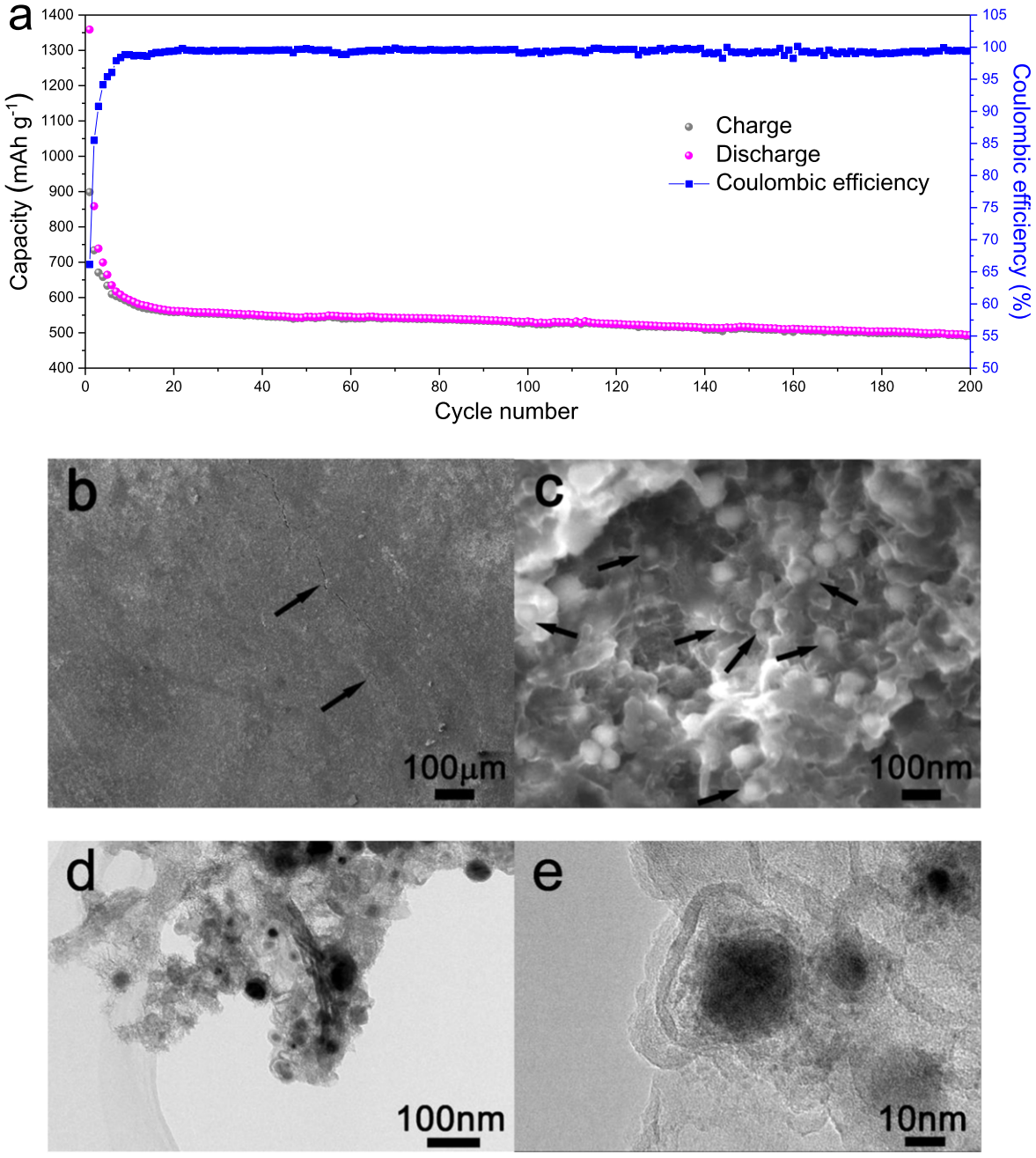


**Figure 8.** (a) The cycling stability and Coulombic efficiency of the $Fe_3O_4$@C anode at a current density of 1 A $g^{-1}$ for 200 cycles; (b), (c) the SEM and (d), (e) the *ex situ* TEM images of the $Fe_3O_4$@C anode after 200 cycles.

core–shell structure are achieved. Otherwise, no extra useless elements are included in the reactants, making that the $Fe_3O_4$@C can be easily collected without tedious purification procedure for eliminating the contaminants. The ferrocene is also abundantly available in China with an affordable price about 6000 dollars per ton, meaning that the raw materials are inexpensive to obtain. For these reasons, the process is very simple, highly efficient and suitable for the large-scale fabrication, which has broad practical applications in industry and commerce.

The electrochemical properties of the $Fe_3O_4$@C anode are provided in figure 7. The first three CV curves of the $Fe_3O_4$@C in figure 7(a) shows a pair of redox peaks located at 0.5 and 1.7 V in the first cycle, respectively. The reduction peak should be ascribed to both the irreversible formation of solid electrolyte interphase (SEI) layer and the lithiation reaction of $Fe_3O_4$ ($Fe_3O_4 + 8Li^+ + 8e \rightarrow Fe^0 + 4Li_2O$), while the oxidation peak comes from the delithiation reaction [16]. In the next two cycles, the CV curves become stable and exhibit good reversibility, implying that the carbon shell can help prevent the surface contact of $Fe_3O_4$ nanocrystals with the electrolyte and protect the interior $Fe_3O_4$ structure. The discharge/charge voltage-capacity profiles at a current density of 100 mA $g^{-1}$ are illustrated in figure 7(b). In the first cycle, the $Fe_3O_4$@C has a flat discharge plateau at 0.85 V with a very high capacity of 1486 mAh $g^{-1}$. As a common

**Table 1.** The literature review of the capacity of pure $Fe_3O_4$ and $Fe_3O_4$@C anode in the voltage of 0–3 V.

| Materials | Current density (mA $g^{-1}$) | Cycle number | Capacity (mAh $g^{-1}$) | References |
|---|---|---|---|---|
| $Fe_3O_4$@C | 100 | 50 | 851 | This work |
| | 500 | 50 | 621 | |
| | 1000 | 200 | 494 | |
| $Fe_3O_4$@nitrogen-doped carbon | 100 | 50 | 848 | [4] |
| Bare $Fe_3O_4$ nanoparticles (20 nm) | 924 | 38 | 260 | [5] |
| $Fe_3O_4$@C | 924 | 50 | 784 | |
| Bare $Fe_3O_4$ nanoparticles (20 nm) | 1000 | 40 | 240 | [17] |
| 3D $Fe_3O_4$@C | 1000 | 50 | 500 | |
| $Fe_3O_4$@C in 2D carbon nanosheet | 1000 | 100 | 998 | |
| Bare $Fe_3O_4$ | 100 | 100 | 93 | [22] |
| $Fe_3O_4$/graphene | 100 | 100 | 650 | |
| $Fe_3O_4$@C | 100 | 50 | 826 | [24] |
| | 500 | 50 | 600 | |
| $Fe_3O_4$@graphene | 900 | 147 | 960 | [25] |
| Hollow $Fe_3O_4$@graphene | 100 | 50 | 900 | [26] |

drawback for the $Fe_3O_4$ anode, the initial Coulombic efficiency is as relatively low as 68%, which is probably associated with the capacity loss during the formation of SEI film and irreversible phase conversion from $Fe_3O_4$ to FeO [17, 18]. The amorphous carbon shell with lots of defects and relatively high surface area also results in the low Coulombic efficiency at the initial stage [19]. But the Coulombic efficiency greatly increases to 95% in the third cycle and remains nearly 100% after the 10th cycle, which suggests a facile lithium insertion/extraction associated with efficient transport of ions and electrons in the $Fe_3O_4$@C anode. The discharge capacities of the $Fe_3O_4$@C at different current densities are displayed in figure 7(c). The capacity can be retained as high as 851 mAh $g^{-1}$ at 100 mA $g^{-1}$ in the 50th cycle. Moreover, the superior reversibility of the $Fe_3O_4$@C is indicated by the almost-horizontal curves after five cycles even at high current densities, and the capacity is equivalent to 471 mAh $g^{-1}$ at 2000 mA $g^{-1}$ after 50 cycles. The rate capabilities of three individual cells are also measured by stepwise increasing the current density from 100 to 2000 mA $g^{-1}$ (figure 7(d)). The capacity suddenly lowers when the current rate is increased and soon becomes stable in the following ten cycles. The three similar curves demonstrate that the microstructure of the $Fe_3O_4$@C is homogeneous. The capacity in the every tenth cycle (red curve) is 800, 649, 473, 360 and 244 mAh $g^{-1}$ using a current density of 100, 200, 500, 1000 and 2000 mA $g^{-1}$, respectively. Additionally, a capacity of 758 mAh $g^{-1}$ is rapidly recovered as the current finally returns back to 100 mA $g^{-1}$. Consequently, the carbon shell is promising for the excellent cyclic capacity retention of the $Fe_3O_4$ anode by stabilizing the microstructure of the $Fe_3O_4$ nanocrystals during the charge/discharge process.

In order to further evaluate the stability of the $Fe_3O_4$@C anode, the long-term cycling performance was carried out at a current density of 1 A $g^{-1}$ for 200 cycles, as shown in figure 8(a). After ten cycles, the discharge capacity of the $Fe_3O_4$@C becomes stable with the value holding at 588 mAh $g^{-1}$ and the corresponding Coulombic efficiency increases up to 98.5%. In the subsequent cycles, the high Coulombic efficiency of nearly 100% is maintained, while the discharge capacity has a slight decay in each cycle and still retains 494 mAh $g^{-1}$ in the 200th cycle. It is indicating that the cycling performance of the $Fe_3O_4$@C anode is very excellent, owing to the good structural stability of the core–shell structure. The morphology of the $Fe_3O_4$@C anode after 200 cycles is also studied by SEM and TEM. In the low magnification SEM image (figure 8(b)), the surface of the anode film is quite smooth and only a few cracks can be observed (indicated by the black arrows) without any peel off from the Cu foil, suggesting that the anode film is sufficiently durable even in the long-term charge/discharge process because the carbon shell can effectively suppress the volume expansion and pulverization of the $Fe_3O_4$ nanocrystals. This can be strongly proved by the large number of core–shell structures (indicated by the black arrows) in the high magnification SEM image (figure 8(c)). Additionally, the *ex situ* TEM analysis was performed, the undamaged core–shell structure can be easily found in the large region image (figure 8(d)). Notably, some hollow cavities between the inner $Fe_3O_4$ core and outer carbon shell are revealed in the high-resolution TEM image (figure 8(e)). The volume expansion of $Fe_3O_4$ is calculated to be 93% under full lithiation [20]. Hence, the carbon shell periodically suffers from tensile stress during the cyclic test, which will be enlarged after long cycles due to the cyclic fatigue damage [21]. Nevertheless, the carbon shell can adequately embrace the $Fe_3O_4$ nanocrystal cores after lithiation and play a major role in maintaining the mechanical and electrical integrity. Considering that there have been many reports on the application of $Fe_3O_4$@C as a cost-effective anode material for lithium-ion batteries, the representative capacities of the pure $Fe_3O_4$ and $Fe_3O_4$@C anodes at different current densities in the voltage of 0–3 V are summarized in table 1. It is well documented that the capacity of bare $Fe_3O_4$ nanoparticles decreases very fast during the course of the initial few cycles, which makes it impossible to be used individually as the anode material

[5, 17, 22]. With the combination of carbon materials, the cyclic stability is greatly improved even in the large current density due to the unchanged morphology of the core–shell structure during the discharge/charge cycles. Owing to the different carbon content in the composite, different capacity values of the $Fe_3O_4$@C anode have been displayed. Most $Fe_3O_4$@C anodes have a capacity of 800–900 and 500–800 mAh $g^{-1}$ after 50 cycles at the current density of 100 and 1000 mA $g^{-1}$, respectively, which are comparable with our results [23]. In addition, to date, this novel one-step preparation procedure for $Fe_3O_4$@C is the simplest and most efficient. The room-temperature carbon encapsulation and scalable preparation are also strong supports for the practical application of the $Fe_3O_4$@C anode.

## 4. Conclusion

The $Fe_3O_4$@C is successfully prepared through the self-propagating reaction of $Cp_2Fe$ with $Fe(NO_3)_3 \cdot 9H_2O$ in the autoclave. The room temperature initiated reaction strongly releases a considerable amount of gas and heat in a short time. The instantaneously raised temperature and pressure in an autoclave will cleave the reactants into small reactive species, which further turns into the core–shell structure. The carbon encapsulation can effectively improve the cycling stability and rate performance of the $Fe_3O_4$. As a result, the method is also desirable for the large-scale preparation of the $Fe_3O_4$@C and will facilitate its potential applications in energy storage and environmental remediation.

## Acknowledgments

This work is sponsored by the Natural Science Foundation of Shanghai (18ZR1417000, 19ZR1422200), the National Natural Science Foundation of China (11572326), the Strategic Priority Research Program of the Chinese Academy of Sciences (XDB22040102), Fundamental Research Funds for the Central Universities of China (2232019G-02) and Opening fund of State Key Laboratory of Nonlinear Mechanics.

## ORCID iDs

Boyang Liu https://orcid.org/0000-0003-1532-7754

## References

[1] Wang H, Chen Q W, Yu Y F, Cheng K and Sun Y B 2011 Size- and solvent-dependent magnetically responsive optical diffraction of carbon-encapsulated superparamagnetic colloidal photonic crystals *J. Phys. Chem.* C **115** 11427–34

[2] Liu R, Guo Y, Odusote G, Qu F and Priestley R D 2013 Core–shell $Fe_3O_4$ polydopamine nanoparticles serve multipurpose as drug carrier, catalyst support and carbon adsorbent *ACS Appl. Mater. Interfaces* **5** 9167–71

[3] Song K, Lee Y, Jo M R, Nam K M and Kang Y-M 2012 Comprehensive design of carbon-encapsulated $Fe_3O_4$ nanocrystals and their lithium storage properties *Nanotechnology* **23** 505401

[4] Ma Y, Zhang C, Ji G and Lee J Y 2012 Nitrogen-doped carbon-encapsulation of $Fe_3O_4$ for increased reversibility in Li+ storage by the conversion reaction *J. Mater. Chem.* **22** 7845–50

[5] Zhao N, Wu S, He C, Wang Z, Shi C, Liu E and Li J 2013 One-pot synthesis of uniform $Fe_3O_4$ nanocrystals encapsulated in interconnected carbon nanospheres for superior lithium storage capability *Carbon* **57** 130–8

[6] Liu B, Ke S, Shao Y, Jia D, Fan C, Zhang F and Fan R 2018 Formation mechanism for oxidation synthesis of carbon nanomaterials and detonation process for core–shell structure *Carbon* **127** 21–30

[7] Liu B, Zhong N, Fan C, Zhou Y, Fan Y, Yu S, Zhang F, Dong L and Yin Y 2014 Low temperature synthesis and formation mechanism of carbon encapsulated nanocrystals by electrophilic oxidation of ferrocene *Carbon* **68** 573–82

[8] Liu B, Fan C, Chen J, Wang J, Lu Z, Ren J, Yu S, Dong L and Li W 2016 Low temperature *in situ* synthesis and the formation mechanism of various carbon-encapsulated nanocrystals by the electrophilic oxidation of metallocene complexes *Nanotechnology* **27** 075603

[9] Nyasulu F W and Mayer J M 1995 Molybdenum oxychlorides I. electrochemistry of $MoO_2Cl_2$: oxidation, dimerization, and electrodeposition at a platinum electrode *J. Electroanal. Chem.* **392** 35–42

[10] Luo K and Dryfe R A W 2009 The formation of silver nanofibres by liquid/liquid interfacial reactions: mechanistic aspects *New J. Chem.* **33** 157–63

[11] Liu B, Shao Y, Xiang X, Zhang F, Yan S and Li W 2017 Highly efficient one-step synthesis of carbon encapsulated nanocrystals by the oxidation of metal $\pi$-complexes *Nanotechnology* **28** 325603

[12] Sutka A and Mezinskis G 2012 Sol-gel auto-combustion synthesis of spinel-type ferrite nanomaterials *Frontiers Mater. Sci.* **6** 128–41

[13] Parnianfar H, Masoudpanah S M, Alamolhoda S and Fathi H 2017 Mixture of fuels for solution combustion synthesis of porous $Fe_3O_4$ powders *J. Magn. Magn. Mater.* **432** 24–9

[14] Manikandan A, Vijaya J J, Mary J A, Kennedy L J and Dinesh A 2014 Structural, optical and magnetic properties of $Fe_3O_4$ nanoparticles prepared by a facile microwave combustion method *J. Ind. Eng. Chem.* **20** 2077–85

[15] Luo N, Li X, Wang X, Yan H, Zhang C and Wang H 2010 Synthesis and characterization of carbon-encapsulated iron/iron carbide nanoparticles by a detonation method *Carbon* **48** 3858–63

[16] Yang Z, Shen J and Archer L A 2011 An *in situ* method of creating metal oxide–carbon composites and their application as anode materials for lithium-ion batteries *J. Mater. Chem.* **21** 11092–7

[17] He C, Wu S, Zhao N, Shi C, Liu E and Li J 2013 Carbon-encapsulated $Fe_3O_4$ nanoparticles as a high-rate lithium ion battery anode material *ACS Nano* **7** 4459–69

[18] Xu Z-L *et al* 2015 *In-situ* TEM examination and exceptional long-term cyclic stability of ultrafine $Fe_3O_4$ nanocrystal/carbon nanofiber composite electrodes *Energy Storage Mater.* **1** 25–34

[19] Wang K, Li Z, Wang Y, Liu H, Chen J, Holmes J and Zhou H 2010 Carbon nanocages with nanographene shell for high-rate lithium ion batteries *J. Mater. Chem.* **20** 9748–53

[20] Qin X, Zhang H, Wu J, Chu X, He Y-B, Han C, Miao C, Wang S, Li B and Kang F 2015 $Fe_3O_4$ nanoparticles encapsulated in electrospun porous carbon fibers with a compact shell as high-performance anode for lithium ion batteries *Carbon* **87** 347–56

[21] Cao K, Li P, Zhang Y, Chen T, Wang X, Zhang S, Liu J and Wang H 2017 *In situ* tem investigation on ultrafast reversible lithiation and delithiation cycling of Sn@C yolk-shell nanoparticles as anodes for lithium ion batteries *Nano Energy* **40** 187–94

[22] Wang J-Z, Zhong C, Wexler D, Idris N H, Wang Z-X, Chen L-Q and Liu H-K 2011 Graphene-encapsulated $Fe_3O_4$ nanoparticles with 3D laminated structure as superior anode in lithium ion batteries *Chem. Eur. J.* **17** 661–7

[23] Zhang Z, Wang F, An Q, Li W and Wu P 2015 Synthesis of graphene@$Fe_3O_4$@C core–shell nanosheets for high-performance lithium ion batteries *J. Mater. Chem.* A **3** 7036–43

[24] Wang J, Zhao H, Zeng Z, Lv P, Li Z, Zhang T and Yang T 2014 Nano-sized $Fe_3O_4$/carbon as anode material for lithium ion battery *Mater. Chem. Phys.* **148** 699–704

[25] Chen Y, Song B, Lu L and Xue J 2013 Ultra-small $Fe_3O_4$ nanoparticle decorated graphene nanosheets with superior cyclic performance and rate capability *Nanoscale* **5** 6797–803

[26] Chen D, Ji G, Ma Y, Lee J Y and Lu J 2011 Graphene-encapsulated hollow $Fe_3O_4$ nanoparticle aggregates as a high-performance anode material for lithium ion batteries *ACS Appl. Mater. Interfaces* **3** 3078–83